



DESIGN AND OPTIMIZATION OF LATTICE STRUCTURES FOR AEROSPACE APPLICATIONS

Enrico Stragiotti

François-Xavier Irisarri¹, Cédric Julien¹ and Joseph Morlier²

1: ONERA - The French Aerospace Lab
DMAS - Département matériaux et structures
92320 Châtillon, France
{francois-xavier.irisarri, cedric.julien}@onera.fr

2: ICA - Institut Clément Ader
ISAE - SUPAERO
31400 Toulouse, France
joseph.morlier@isae-supraero.fr
November 7, 2023

PhD manuscript

ONERA – ISAE Supaero

Colophon

This document was typeset with the help of KOMA-Script and L^AT_EX using the kaobook class.

ONERA – ISAE Supaero

CONTENTS

Contents	iii
List of Figures	v
List of Tables	v
List of Abbreviations	v
1 Optimizing modular structures	1
1.1 Formulation of a modular structure optimization algorithm	1
1.1.1 Variable linking	2
1.1.2 Topological buckling of modular structures	3
1.1.3 Optimization formulation	3
1.1.4 Sensitivity analysis	4
1.2 Numerical application	5
1.2.1 On the equivalence of multi load cases and modular structures	5
1.2.2 Parametric study on the number, the shape, and the complexity of the module	6
1.2.3 Comparison with the optimized octet truss	11
1.2.4 Using multiple module's topologies	12
1.3 Conclusion	17
Bibliography	19

LIST OF FIGURES

1.1	Notations used for the definition of the variable linking approach used to apply the modularity constraints.	1
1.2	Notations used for the definition of the variable linking approach used to apply the modularity constraints.	5
1.3	6
1.4	spiega colori as usual	6
1.5	8
1.6	(a-d) (e-h) add 30	9
1.7	metti undeformed	9
1.8	(a-d) (e-h)	9
1.9	10
1.10	limited to 500 and 2e5	12
1.11	12
1.12	todo	13
1.13	todo	14
1.14	14
1.15	15
1.17	todo	15
1.16	17

LIST OF TABLES

1.1	Material data used for the simply supported 3D beam optimization.	5
1.2	6
1.3	Material data used for the simply supported 3D beam optimization.	7
1.4	7
1.5	10
1.6	Volume	11
1.7	Time	11
1.8	14
1.9	16

LIST OF ABBREVIATIONS

RVE Representative Volume Element

TTO Truss Topology Optimization

OPTIMIZING MODULAR STRUCTURES

Introduction change N_T con N_T NO CELLS metti slend min sulle barre tables always small

1.1 FORMULATION OF A MODULAR STRUCTURE OPTIMIZATION ALGORITHM	1
1.2 NUMERICAL APPLICATION	5
1.3 CONCLUSION	17

1.1 FORMULATION OF A MODULAR STRUCTURE OPTIMIZATION ALGORITHM

Assembled modular ultralight structures present an opportunity to greatly improve the performance and cost efficiency of modern aerostructures [1]. The repetitive nature brings various interesting features among which reduced tooling, fast assembly, and short repair time. Additionally, as the mechanical performance of the structure is greatly influenced by the topology and the materials of the repetitive pattern, modular structures are naturally prone to optimization.

In the structure optimization field periodic materials are often modeled by means of asymptotic homogenization [2]. The heterogeneous module topology (also called Representative Volume Element (RVE)) is treated as homogeneous material with associated mechanical properties i.e. equivalent elastic tensor, shear modulus, etc. The homogenization approach is valid only if the RVE contains enough information about the heterogeneous material and if the structure presents significant periodicity [3, 4]. When designing modular structures (and not materials), no scale separation is assumed between the repetitive pattern and the structure itself. Consequently, the hypotheses of asymptotic homogenization are not always verified. For that reason, full-scale approaches [5] have been developed.

1. Cramer et al. (2019), 'Elastic shape morphing of ultralight structures by programmable assembly'

2. Zhou et al. (2008), 'Design of graded two-phase microstructures for tailored elasticity gradients'

3. Kalamkarov et al. (2009), 'Asymptotic Homogenization of Composite Materials and Structures'

4. Li et al. (2020), 'Anisotropic design and optimization of conformal gradient lattice structures'

5. Wu et al. (2021), 'Topology optimization of multi-scale structures'

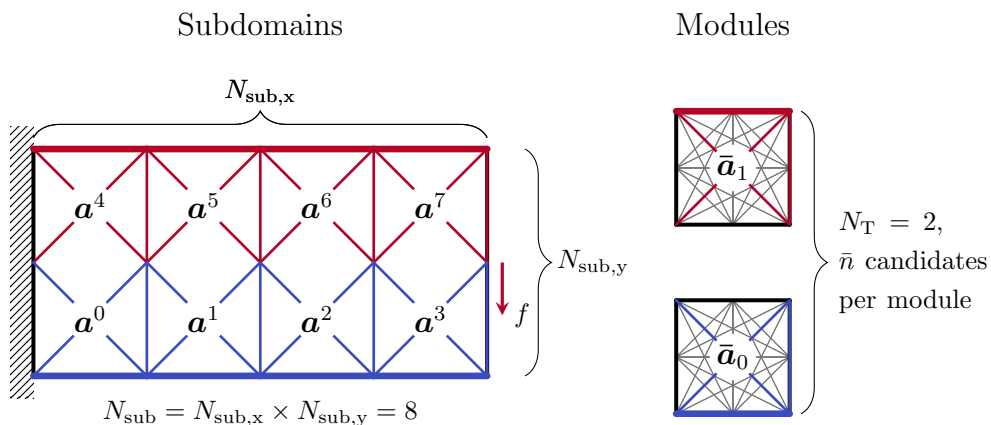


Figure 1.1: Notations used for the definition of the variable linking approach used to apply the modularity constraints.

6. Zhang et al. (2006), 'Scale-related topology optimization of cellular materials and structures'

1.1.1 VARIABLE LINKING

The variable linking approach [6] is a full-scale technique that involves first dividing a structure into several subdomains, which are connected during the optimization process i.e. subdomains that belong to the same module all share the same cross-sectional areas. The primary goal is to make the manufacturing phase simpler and more efficient, allowing to assemble big structures starting from smaller repetitive modules. With this approach, the optimization perspective shifts. The optimizer design space using the variable linking approach is restricted to the optimization of the topology of the modules, using the whole structure just to impose the necessary mechanical constraints.

We use Fig. 1.1 to illustrate the notation employed in this thesis for modular structures. On the left-hand side of the image, we have the whole test case that we aim to optimize, which is already divided into N_{sub} subdomains. Each of these subdomains is bound to exhibit the topology of one of the N_T module topologies presented on the right side of the image. It is assumed that each module has the same external shape and the identical ground structure used for discretizing the module volume. Within this framework, \bar{n} represents the number of candidate bars in one module, and if we assume a fully connected mesh, we can define $\bar{n} = \bar{m} \cdot (\bar{m} - 1)/2$, where \bar{m} stands for the number of nodes in the module. Consequently, for the overall structure, we can write the relationship $N_{\text{el}} = N_{\text{sub}}\bar{n}$.

The vector that holds all the cross-sectional areas of the modules is represented by $\bar{\mathbf{a}}$, and it belongs to the set of positive real numbers $\mathbb{R}_+^{N_T \cdot \bar{n}}$. This vector is essentially a grouping of individual cross-sectional areas $\bar{\mathbf{a}}_t$ for each of the N_T modules. In mathematical terms, $\bar{\mathbf{a}}$ is defined as follows:

$$\bar{\mathbf{a}} := \{\bar{\mathbf{a}}_t \in \mathbb{R}_+^{\bar{n}} \mid \forall t \in [1, \dots, N_T]\} \quad (1.1)$$

In the case of the structure shown in Fig. 1.1 we have:

$$H = \begin{array}{cc|c} t=0 & t=1 & \\ \hline 1 & 0 & j=0 \\ 1 & 0 & j=1 \\ 1 & 0 & j=2 \\ 1 & 0 & j=3 \\ 0 & 1 & j=4 \\ 0 & 1 & j=5 \\ 0 & 1 & j=6 \\ 0 & 1 & j=7 \end{array} \quad (1.4)$$

as the lower submodules (numbered from 0 to 3) exhibit the topology of module $t = 0$, while the upper submodules (numbered 4 to 7) the topology of module $t = 1$.

The topology of the entire structure \mathbf{a} , which originates from the submodules' topology $\bar{\mathbf{a}}$, is defined as follows:

$$\mathbf{a} := \{\mathbf{a}^j \mid \forall j \in [1, \dots, N_{\text{sub}}]\} \quad (1.2)$$

and is evaluated using:

$$\mathbf{a} = \sum_{t=1}^{N_T} \mathbf{G}_t \otimes \bar{\mathbf{a}}_t = \sum_{t=1}^{N_T} \begin{bmatrix} h_{1,t} & \bar{\mathbf{a}}_t \\ \vdots & \\ h_{N_{\text{sub}},t} & \bar{\mathbf{a}}_t \end{bmatrix} \quad (1.3)$$

where the \otimes operator represents the Kronecker product and \mathbf{h}_t is the t -th column of the mapping matrix $\mathbf{H} = [\mathbf{h}_0, \dots, \mathbf{h}_{N_T}] \in \mathbb{B}^{N_{\text{sub}}, N_T}$, where $\mathbb{B} = \{0, 1\}$ is the Boolean domain. $G_{j,t}$ is the element at the j -th row and t -th column of the matrix \mathbf{H} . The mapping matrix \mathbf{H} indexes are defined as follows:

$$G_{j,t} = \begin{cases} 1 & \text{if the } j\text{-th subdomain presents the topology of the } t\text{-th module,} \\ 0 & \text{otherwise.} \end{cases} \quad (1.5)$$

Lastly, we introduce some notation to denote specific bars within the modules and subdomains. We represent the cross-sectional area of the i -th bar of the t -th module as $\bar{a}_{t,i}$, while the cross-sectional area of the i -th bar of the j -th subdomain as a_i^j .

1.1.2 TOPOLOGICAL BUCKLING OF MODULAR STRUCTURES

Addressing topological buckling in modular structures is a more complex task compared to monolithic structures. This complexity arises from the fact that we must not only consider bars within a single module's design space but also those connecting different modules. Since the nature of this problem heavily relies on how the modules are arranged within the structure, we have opted for a simplification. We focus only on the assessment of nodal instability within each module, modifying the length ℓ^* used to evaluate the critical buckling force of ?? and Equation ?? only of compressive chains of bars that fall inside a module. Additionally, Equation ?? is modified as follows:

$$\bar{a}_{t,r} \geq \bar{a}_{t,r=1} \quad r \in \mathcal{C}_{l,r}(\bar{a}_t) \quad \forall t \in [1, \dots, N_T]. \quad (1.6)$$

We have made this choice knowing that the high connectivity of modular structures tends to reduce the occurrence of nodal instability within the structure. Any potential nodal instability in compressive chains at the structure level is addressed in a subsequent post-processing phase.

1.1.3 OPTIMIZATION FORMULATION

Monolithic formulation ?? is modified using Equations 1.3, and 1.6 to obtain the modular optimization formulation \mathbb{M}_1 that use the variable linking approach. Formulation \mathbb{M}_1 is stated in terms of modular cross-sectional areas \bar{a} , member forces q and nodal displacements U as follows:

$$\begin{aligned} \min_{\bar{a}, q, U} \quad & V = \ell^T a \\ \text{s.t.} \quad & a = \sum_{t=1}^{N_T} h_t \otimes \bar{a}_t \\ & Bq = f \\ & q = \frac{aE}{\ell} b^T U \\ & q \geq -\frac{sa^2}{\ell^{*2}} \\ & -\sigma_c a \leq q \leq \sigma_t a \\ & \bar{a}_{t,r} \geq \bar{a}_{t,r=1} \quad r \in \mathcal{C}_{l,r}(\bar{a}_t), \forall t \end{aligned} \quad (\mathbb{M}_1)$$

The total number of constraints of the formulation is $N_T \bar{n} + N_{\text{sub}} \bar{n} + 2M$ or $N_T \bar{n} + N_{\text{sub}} \bar{n} + 3M$ in function of the test case is two or three dimensional. The number of constraints is, however, equal to the monolithic optimization, as stress, buckling and compatibility are all local grandeurs and are then referenced to the whole structure and not only the modules.

The formulation is solved applying the two step optimization algorithm with the use of the reinitialization heuristic to reduce the dependence to the starting point proposed in Section ??, for that reason we state the relaxed formulation m2 that is solved instead of m1 to

$$\begin{aligned}
 \min_{\bar{\alpha}, q, U} \quad & V = \ell^T \alpha \\
 \text{s.t.} \quad & \alpha = \sum_{t=1}^{N_T} h_t \otimes \bar{a}_t \\
 & Bq = f \\
 & q \geq -\frac{s \alpha^2}{\ell^{*2}} \\
 & -\sigma_c \alpha \leq q \leq \sigma_t \alpha \\
 & \bar{a}_{t,r} \geq \bar{a}_{t,r=1} \quad r \in \mathcal{C}_{l,r}(\bar{a}_t), \forall t \\
 & \bar{a} \geq 0.
 \end{aligned} \tag{M2}$$

Formulation m2 is solvable using a succession of linearized problem using a SLP algorithm. this is possible because the kronecker product is a linear operator and buckling constraints are linearized as already done on Section ??

1.1.4 SENSITIVITY ANALYSIS

how the sensitivity is changed with respect to the variable linking just a sum more to do for constraints

the idea is that we first evaluate all the gradients for all the candidates as there are no modularity constraints. then we sum the apport of every i -th bar that belongs to a single module topology t together.

mathematically we can write that the result is a scalar

$$\frac{\partial(\cdot)_i}{\partial \bar{a}_{t,i}} = \sum_{j=0}^{N_{\text{sub}}} h_t^T \frac{\partial(\cdot)_i}{\partial a_i^j} \tag{1.7}$$

where (\cdot) is a function **image for sensitivity ?**

put dotted lines on the modules

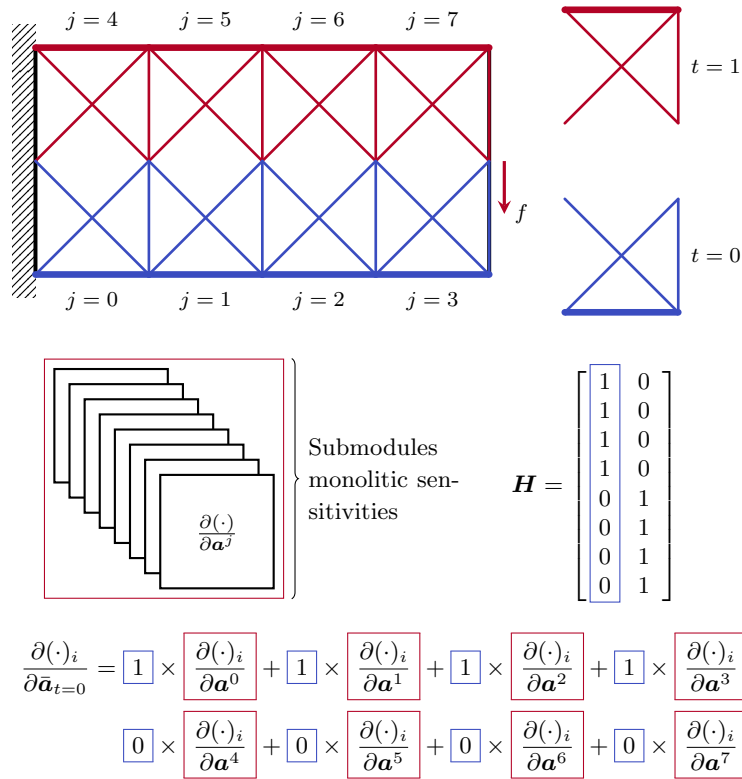


Figure 1.2: Notations used for the definition of the variable linking approach used to apply the modularity constraints.

1.2 NUMERICAL APPLICATION

find some litterature case that we can use to compare at least visually, maybe the sandwich structure that joseph suggested me

1.2.1 ON THE EQUIVALENCE OF MULTI LOAD CASES AND MODULAR STRUCTURES

The first test case we optimize is a section of bridge structure made by two submodules and with symmetric BCs as shown in fig xx a. two vertical loads are applied in the lower side of the design space as shown in fig xx. the material and geometrical data are presented in Tab xx. Tevery subdomain of the structure is discretized using a 15x15 fully connected ground structure. buckling constraints are turned off in this example. alongside the presented test case, we optimize another similar structure, this time made by only a single submodule loaded with two different load cases p1 and p2, positioned at exactly the same distance from the support (see fig xx b) table results add lenght for the loads, so the reader understands

we optimized the two load cases using $p = 0.05$ for the first case and $p = 0.1$ for the second. we get exactly the same topology with vol V1 = 2V2. this simple example mette in luce an interesting property of the optimization of modular structures that could have been theorized only using common sense. when a loaded structure is subdivided

Parameter	Value
L	100
E	1
σ_c, σ_t	± 1
P	1

Table 1.1: Material data used for the simply supported 3D beam optimization.

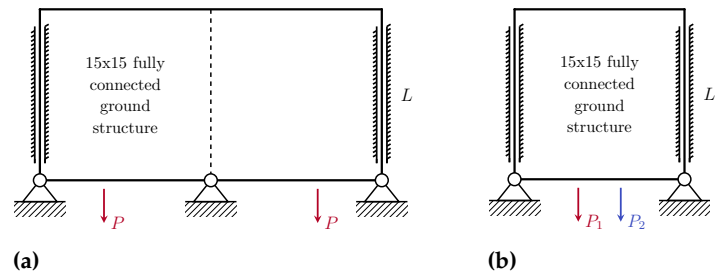


Figure 1.3

Table 1.2

Quantity	6x2x3	
	Octet	3x3x3
N_{sub}	36	36
$N_{\text{opt}} (N_{\text{el}})$	1008	468 (12636)
V		
V^*		

in multiple subdomains, every one subdomain, if isolated from the structure and applying the correct boundary conditions made by the reaction forces of the adjacent bars and supports, is subject to different loading conditions. If then we apply some modularity constraints to all of these modules, we are looking for the best structure that optimizes contemporaneously all of these different load cases.

Furthermore, these examples confirm us that when dealing with modularity constraints, we need to solve the *quindi conferma del bisogno di usare l nlp con i kinematic constraints*

1.2.2 PARAMETRIC STUDY ON THE NUMBER, THE SHAPE, AND THE COMPLEXITY OF THE MODULE

IN this section we set up a parametric study on the scale and on the complexity of the module used for optimizing the . we do not study yet the effect that it has to have multiple module topologies

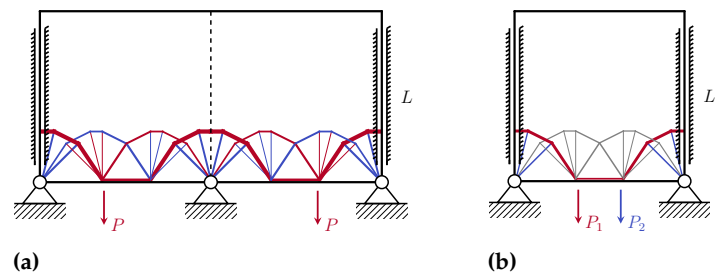


Figure 1.4: spiega colori as usual

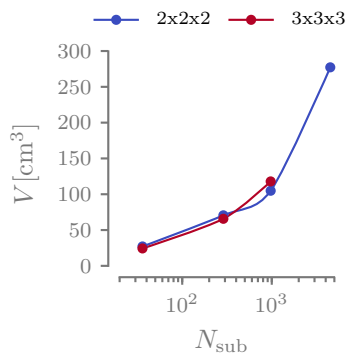
Scale effect of the square RVE on the design results: add here the monolith **il caso 30x mostra un lamda ridicolo, scrivilo, metti che hai messo 10**

Parameter	Value
E	2.7 GPa
ν	0.3
σ_c, σ_t	± 55 MPa
ρ	1.14 g cm^{-3}
P	100 N

Table 1.3: Material data used for the simply supported 3D beam optimization.

Table 1.4

Quantity	7x3x4	2x2x2				3x3x3		
	1x1x1	6x2x3	12x4x6	18x6x9	30x10x15	6x2x3	12x4x6	18x6x9
$\bar{n}_{\text{opt}} (\bar{n})$	1984	9 (28)	9 (28)	8 (28)	8 (28)	19 (351)	15 (351)	16 (351)
N_{sub}	1	36	288	972	4500	36	288	972
$N_{\text{opt}} (N_{\text{el}})$	20 (1984)	324 (1008)	2592 (8064)	7776 (27216)	36000 (126000)	468 (12636)	4320 (101088)	15552 (341172)
$V [\text{cm}^3]$	9.907	27.074	70.559	104.891	277.238	24.323	65.723	117.904
$V [\%]$	1.761	4.812	12.544	18.648	49.288	4.324	11.684	20.960
$C [\text{J}]$	3.71	4.22	3.35	3.19	1.12	3.63	1.84	2.02
$a_{\text{max}} [\text{mm}^2]$	37.61	9.40	5.45	5.45	3.55	5.33	2.60	3.14
t	4 s	6 s	48 s	5 m 6 s	1 h 17 m	5 m 42 s	42 m 50 s	27 h 17 m

**Figure 1.5**

in the last one the buckling length is so small that stress equals compressive and tensile failure

the inefficiency can be observed for example having q look at figure xx where the stress and buckling constraints activate only on one submodules but force the whole structure to show it quand même

Effects of the aspect ratio of the RVE on the design results

Effects of the complexity of the

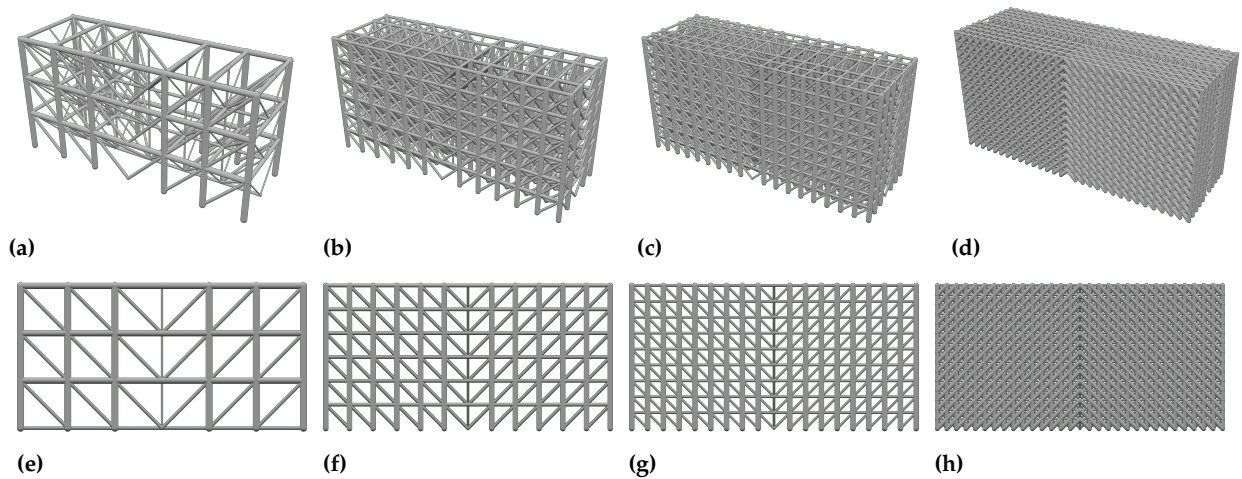


Figure 1.6: (a-d) (e-h) add 30

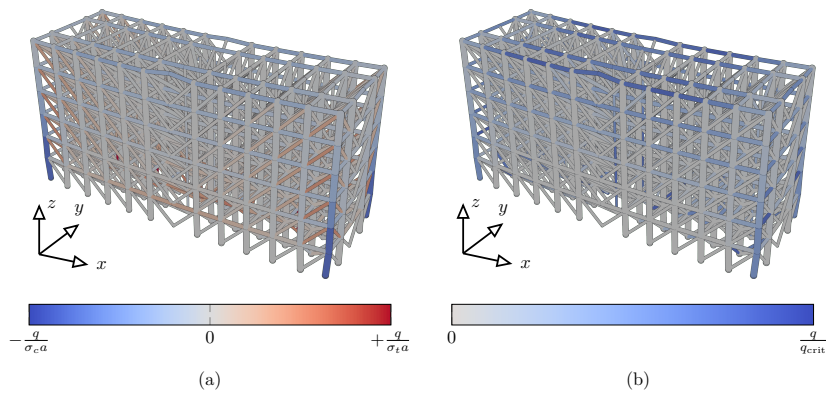


Figure 1.7: metti undefined

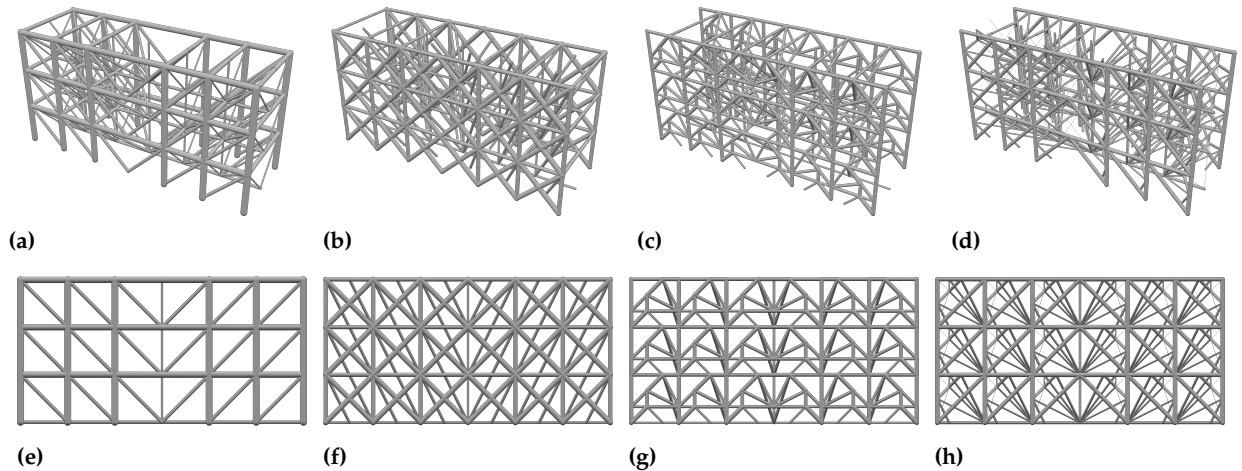


Figure 1.8: (a-d) (e-h)

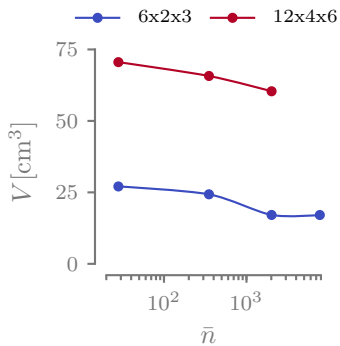


Figure 1.9

use blender to generate images

check always the number of design variables, constraints and time

devirendere i dati digesti, gare dei grafici di riepilogo delle cose interessanti. le tab servono da database ma non servono per spiegare

different tables for every parametric study with iteration count

name, table with number of candidates per module, number of subdomain and calculation time

doe with calc time and volume Simply supported 3D beam

fai il doe we limit to cubic cell for semplicity here are the outcomes

$$a x_1^2 + b x_2^2 + c x_1 x_2 + d x_1 + e x_2 + f \quad (1.8)$$

Table 1.5

Quantity	6x2x3				12x4x6		
	2x2x2	3x3x3	4x4x4	5x5x5	2x2x2	3x3x3	4x4x4
$\bar{n}_{\text{opt}} (\bar{n})$	9 (28)	19 (351)	88 (2016)	88 (7750)	9 (28)	15 (351)	22 (2016)
N_{sub}	36	36	36	36	288	288	288
$N_{\text{opt}} (N_{\text{el}})$	324 (1008)	468 (12636)	792 (72576)	792 (279000)	2592 (8064)	4320 (101088)	6336 (580608)
$V [cm^3]$	27.074	24.323	17.098	17.083	70.559	65.723	60.368
$V [\%]$	4.812	4.324	3.040	3.036	12.544	11.684	10.732
$C [J]$	4.22	3.63	4.49	3.91	3.35	1.84	2.43
$a_{\max} [\text{mm}^2]$	9.40	5.33	3.39	3.77	5.45	2.60	2.97
t	6 s	5 m 42 s	14 m 20 s	3 h 17 m	48 s	42 m 50 s	32 h 4 m

1.2.3 COMPARISON WITH THE OPTIMIZED OCTET TRUSS

The Truss Topology Optimization (TTO) algorithm is here benchmarked against one of the most popular cell topologies present in the literature: the octet-truss (see Fig. xx). The octet-truss is a cell known for having very good effective mechanical properties that attain about half the theoretical values of the upper Hashi-Shtrikman bounds [7].

To perform the benchmark, the wing box of Figure xx is meshed using $44 \times 4 \times 1$ octet-truss cells of 125 mm of edge size (see Fig. xx). The cross-sectional areas of the cell members are all equal. The section value is evaluated by performing a parametric optimization on this section value, constrained by stress and local buckling for every member of the structure. The optimization is performed using Altair OptiStruct.

Coeff.	Value
a	9.00×10^{-8}
b	-1.02×10^{-5}
c	-1.77×10^{-6}
d	-2.64×10^{-3}
e	1.01×10^{-1}
f	2.88×10^1

Table 1.6: Volume

Coeff.	Value
a	1.55×10^{-3}
b	-2.87×10^{-4}
c	2.90×10^{-1}
d	-2.08×10^1
e	-5.54
f	0.00

Table 1.7: Time

[7] Deshpande et al. (2001), 'Effective properties of the octet-truss lattice material'

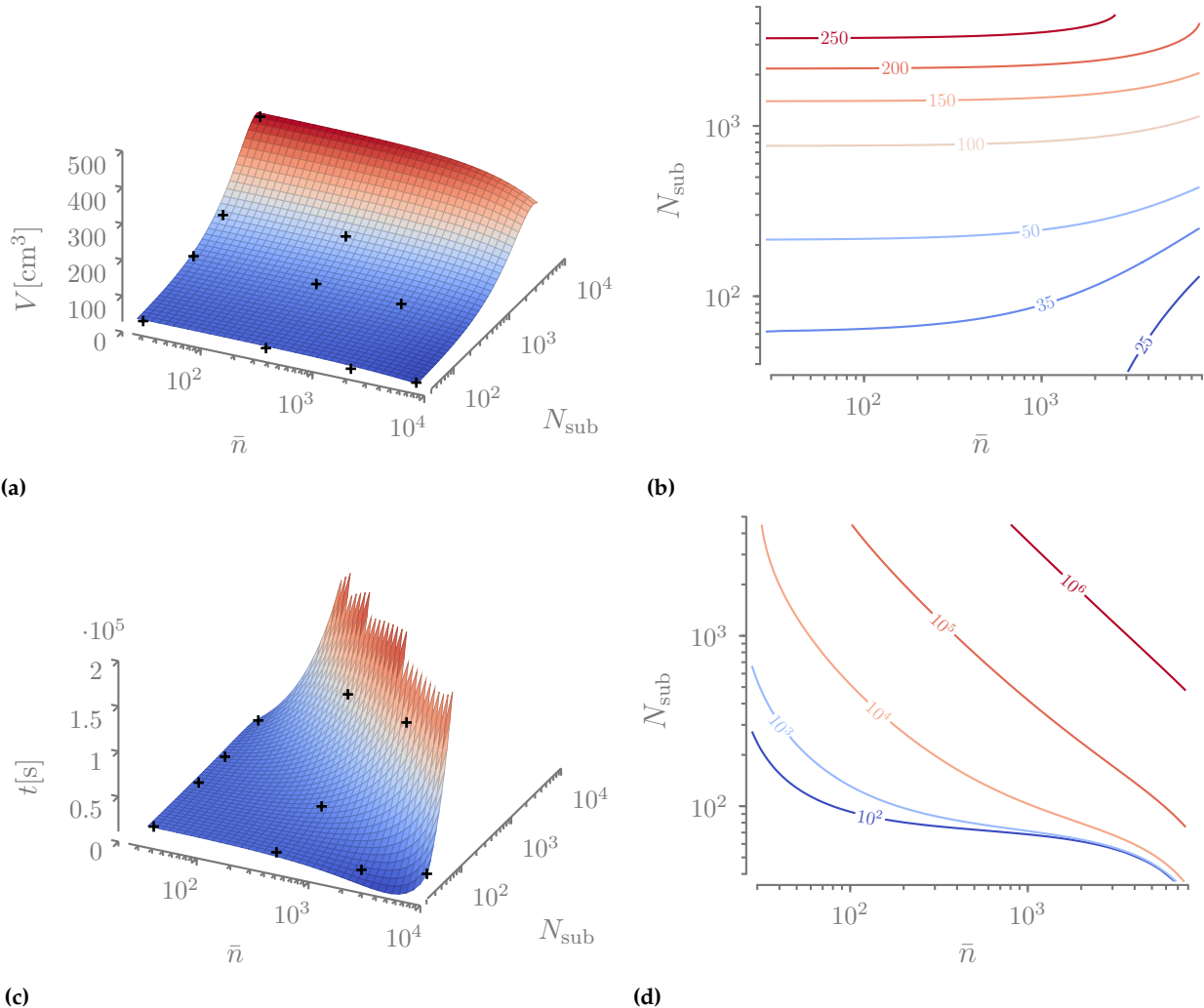


Figure 1.10: limited to 500 and 2e5

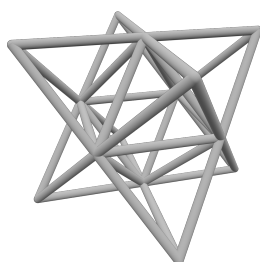


Figure 1.11

1.2.4 USING MULTIPLE MODULE'S TOPOLOGIES

this study suggest that we have here a compromise between volume (and then mass) and manufacturing complexity. we studied till now the two extremities, the full modular and the monolithic structure. we want now to see what happens in between

$$H = \begin{bmatrix} 1 & 0 & 0 \\ 1 & 0 & 0 \\ 1 & 0 & 0 \\ 0 & 0 & 0 \\ 0 & 1 & 0 \\ 0 & 1 & 0 \\ 0 & 1 & 0 \\ 0 & 0 & 1 \\ 0 & 0 & 1 \\ 0 & 0 & 1 \end{bmatrix}$$

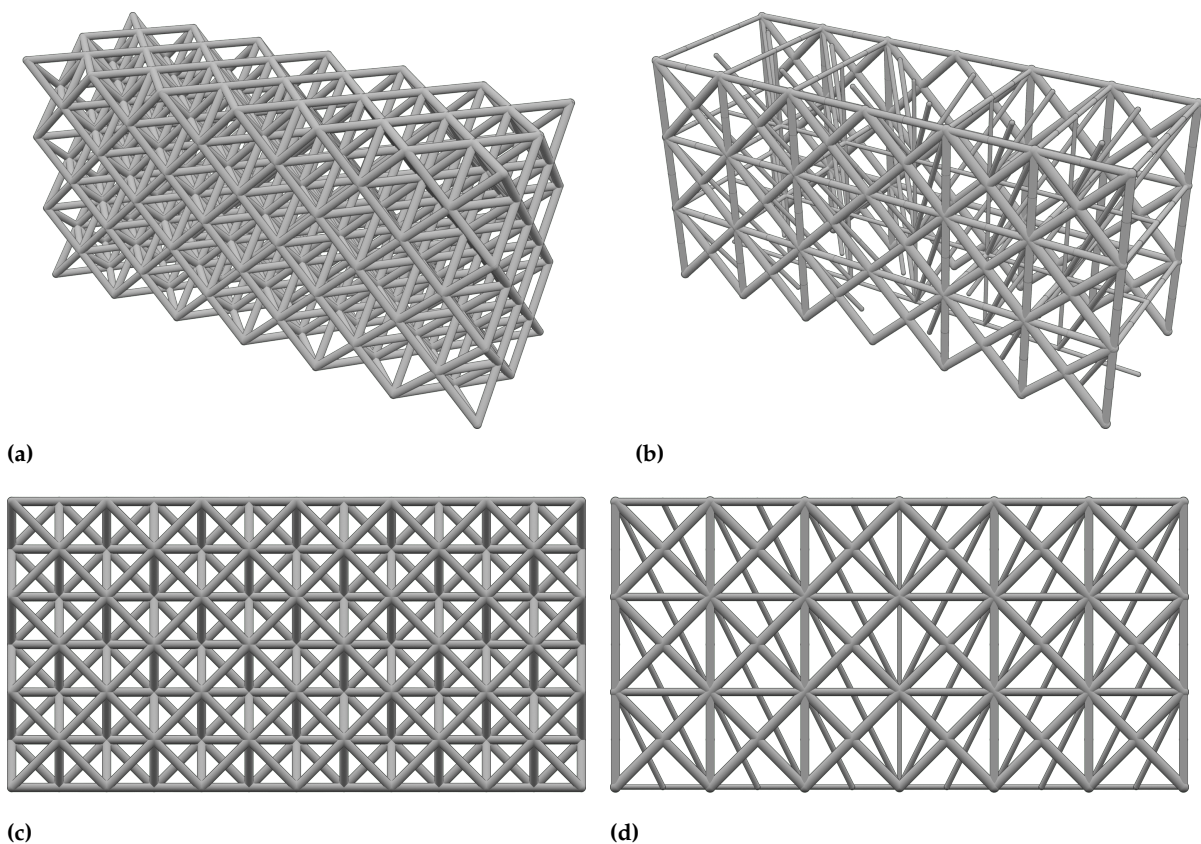


Figure 1.12: todo

show a picture that the design is more stressed compared to before

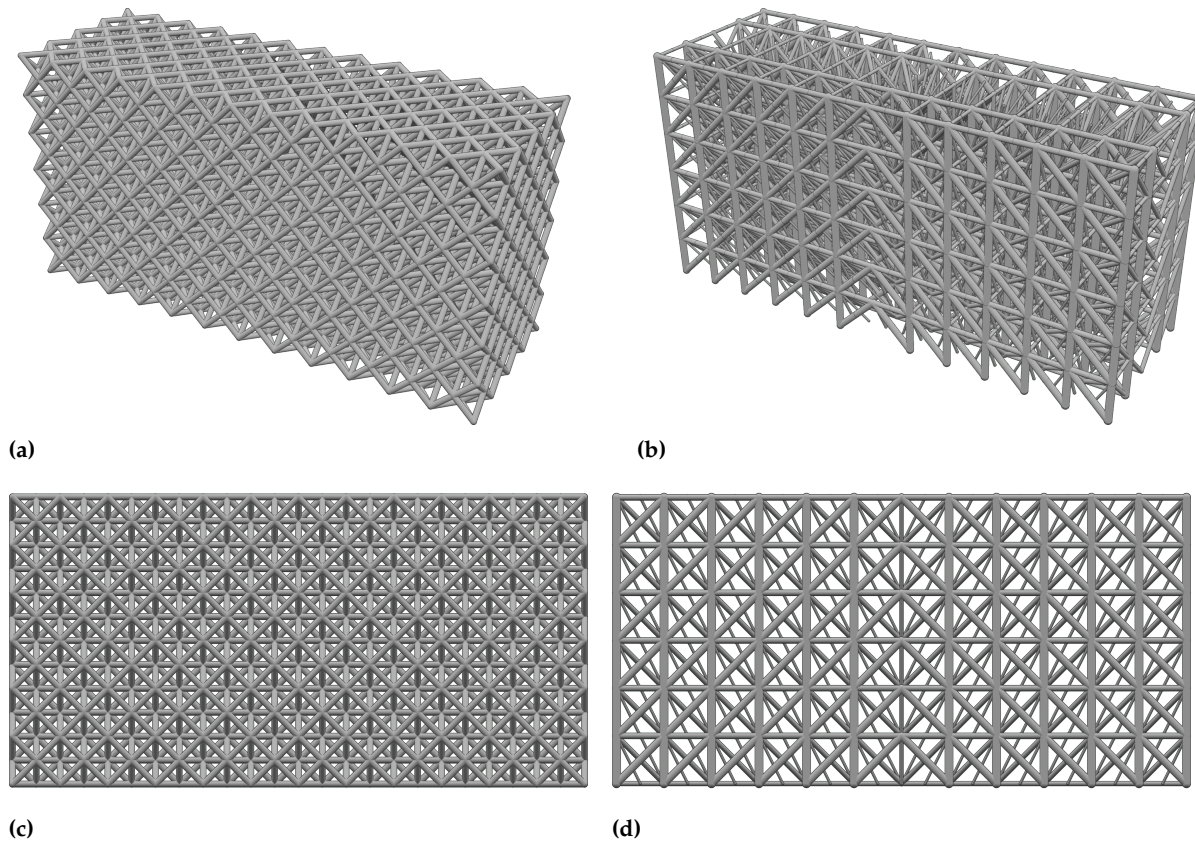


Figure 1.13: todo

Table 1.8

Quantity	6x2x3		12x4x6	
	Octet	3x3x3	Octet	3x3x3
N_{sub}	36	36	288	288
$N_{\text{opt}} (N_{\text{el}})$	1008	468 (12636)	7488	4320 (101088)
$V [\text{cm}^3]$	65.752	24.323	121.038	65.723
$V [\%]$	11.692	4.324	21.524	11.684
$C [\text{J}]$	1.67	3.63	1.12	1.84
$a_{\max} [\text{mm}^2]$	3.69	5.33	1.83	2.60

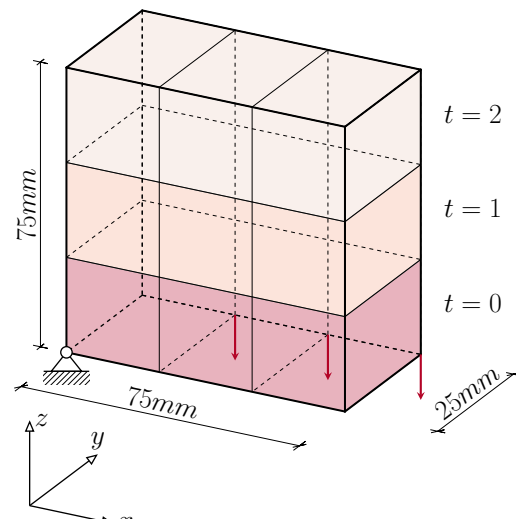


Figure 1.14

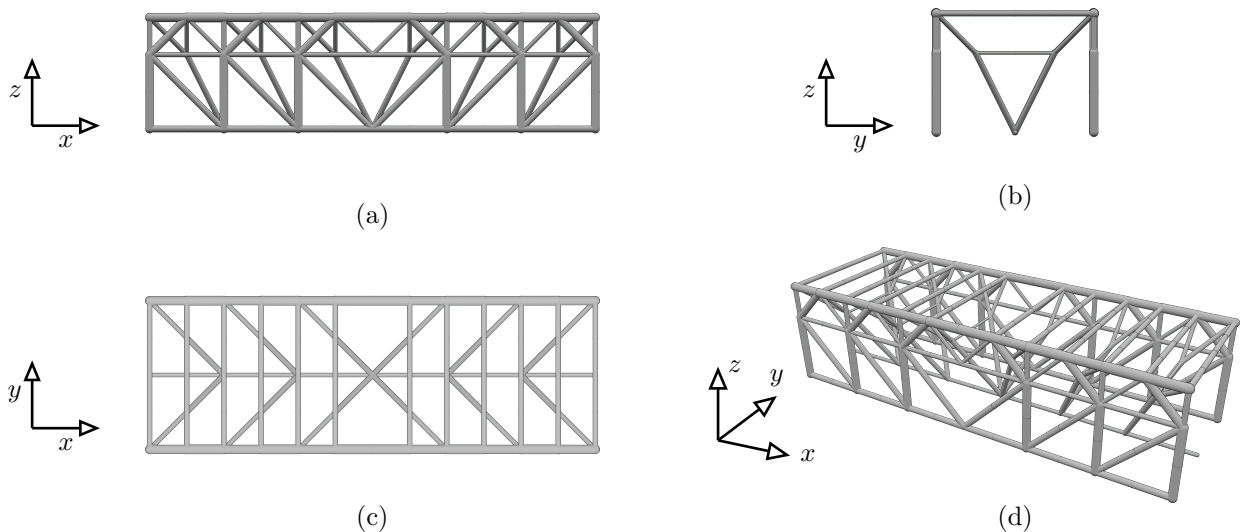


Figure 1.15

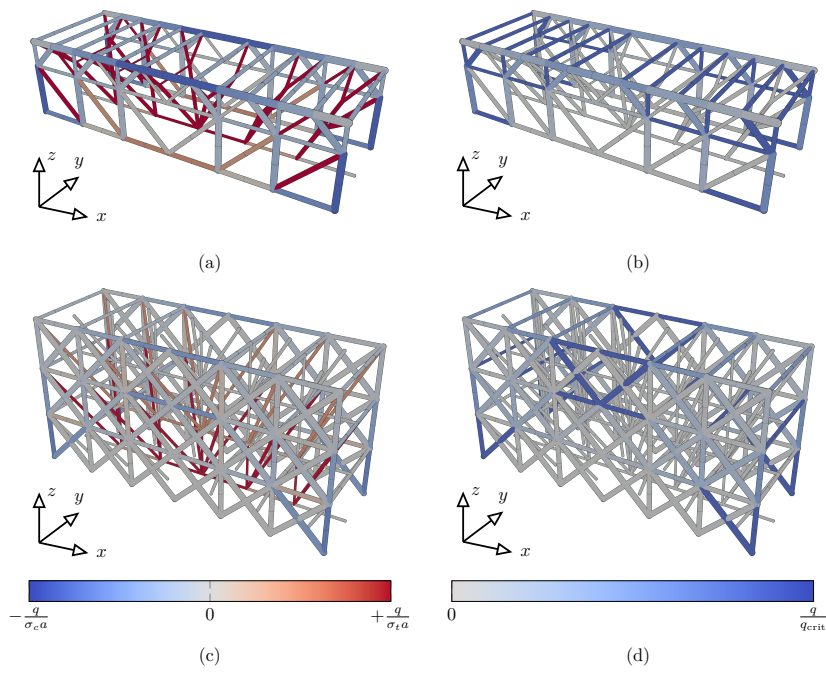
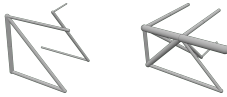


Figure 1.17: todo

Table 1.9

Quantity	7x3x4	6x2x3 $N_t = 3$			6x2x3 $N_t = 1$
	-	$t = 0$	$t = 1$	$t = 2$	$t = 0$
	-			-	
$\bar{n}_{\text{opt}} (\bar{n})$	1984	10 (351)	18 (351)	- (351)	19 (351)
N_{sub}	1		36		36
$N_{\text{opt}} (N_{\text{el}})$	20 (1984)		336 (12636)		468 (12636)
V [cm ³]	9.907		12.032		24.323
V [%]	1.761		2.139		4.324
C [J]	3.71		6.14		3.63
a_{\max} [mm ²]	37.61		7.13		5.33
t	4 s		3 m 22 s		5 m 42 s

1.3 CONCLUSION

It's all part of our effort to strike a balance between mechanical performance and the ease of manufacturing, a topic we'll delve into further in the upcoming chapters.

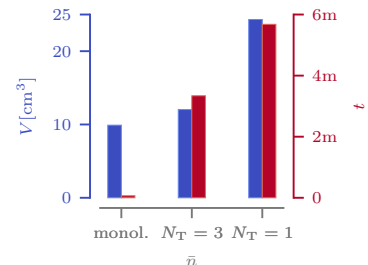


Figure 1.16

BIBLIOGRAPHY

- [1] Cramer, Nicholas B., Cellucci, Daniel W., Formoso, Olivia B., Gregg, Christine E., Jenett, Benjamin E., Kim, Joseph H., Lendraitis, Martynas, Swei, Sean S., Trinh, Greenfield T., Trinh, Khanh V., and Cheung, Kenneth C., 'Elastic shape morphing of ultralight structures by programmable assembly', *Smart Materials and Structures* 28.5 (Apr. 2019), p. 055006.
doi: [10.1088/1361-665X/ab0ea2](https://doi.org/10.1088/1361-665X/ab0ea2) cited on page 1
- [2] Zhou, Shiwei and Li, Qing, 'Design of graded two-phase microstructures for tailored elasticity gradients', *Journal of Materials Science* 43.15 (Aug. 2008), pp. 5157–5167.
doi: [10.1007/s10853-008-2722-y](https://doi.org/10.1007/s10853-008-2722-y) cited on page 1
- [3] Kalamkarov, Alexander L., Andrianov, Igor V., and Danishevskyy, Vladyslav V., 'Asymptotic Homogenization of Composite Materials and Structures', *Applied Mechanics Reviews* 62.3 (Mar. 2009).
doi: [10.1115/1.3090830](https://doi.org/10.1115/1.3090830) cited on page 1
- [4] Li, Dawei, Liao, Wenhe, Dai, Ning, and Xie, Yi Min, 'Anisotropic design and optimization of conformal gradient lattice structures', *Computer-Aided Design* 119 (Feb. 2020), p. 102787.
doi: [10.1016/j.cad.2019.102787](https://doi.org/10.1016/j.cad.2019.102787) cited on page 1
- [5] Wu, Jun, Sigmund, Ole, and Groen, Jeroen P., 'Topology optimization of multi-scale structures: a review', *Structural and Multidisciplinary Optimization* (Mar. 2021).
doi: [10.1007/s00158-021-02881-8](https://doi.org/10.1007/s00158-021-02881-8) cited on page 1
- [6] Zhang, Weihong and Sun, Shiping, 'Scale-related topology optimization of cellular materials and structures', *International Journal for Numerical Methods in Engineering* 68.9 (2006), pp. 993–1011.
doi: [10.1002/nme.1743](https://doi.org/10.1002/nme.1743) cited on page 2
- [7] Deshpande, V. S., Fleck, N. A., and Ashby, M. F., 'Effective properties of the octet-truss lattice material', *Journal of the Mechanics and Physics of Solids* 49.8 (Aug. 2001), pp. 1747–1769.
doi: [10.1016/S0022-5096\(01\)00010-2](https://doi.org/10.1016/S0022-5096(01)00010-2) cited on page 11

